ORIGINAL CONTRIBUTION

Cononsolvency of the responsive polymer poly(*N*-isopropylacrylamide) in water/methanol mixtures: a dynamic light scattering study of the effect of pressure on the collective dynamics

Bart-Jan Niebuur[1,2] · André Deyerling[1,3] · Nicole Höfer[1,4] · Alfons Schulte[5] · Christine M. Papadakis[1]

Abstract

The collective dynamics of 25 wt% poly(*N*-isopropylacrylamide) (PNIPAM) solutions in water or an 80:20 v/v water/methanol mixture are investigated in the one-phase region in dependence on pressure and temperature using dynamic light scattering. Throughout, two dynamic modes are observed, the fast one corresponding to the relaxation of the chain segments within the polymer blobs and the slow one to the relaxation of the blobs. A pressure scan in the one-phase region on an aqueous solution at 34.0 °C, i.e., slightly below the maximum of the coexistence line, reveals that the dynamic correlation length of the fast mode increases when the left and the right branch of the coexistence line are approached. Thus, the chains are rather swollen far away from the coexistence line, but contracted near the phase transition. Temperature scans of solutions in neat H_2O or in H_2O/CD_3OD at 0.1, 130, and 200 MPa reveal that the dynamic correlation length of the fast mode shows critical behavior. However, the critical exponents are significantly larger than the value predicted by mean-field theory for the static correlation length, $\nu = 0.5$, and the exponent is significantly larger for the solution in the H_2O/CD_3OD mixture than in neat H_2O.

✉ Alfons Schulte
alfons.schulte@ucf.edu

✉ Christine M. Papadakis
papadakis@tum.de

[1] Physik-Department, Fachgebiet Physik Weicher Materie, Technische Universität München, James-Franck-Straße 1, Garching 85748, Germany

[2] Present Address: INM - Leibniz Institute for New Materials, Campus D2 2, Saarbrücken 66123, Germany

[3] Present Address: Physik-Department, Lehrstuhl Für Topologie Korrelierter Systeme, Technische Universität München, James-Franck-Str. 1, Garching 85748, Germany

[4] Present Address: Fachbereich Physik, AG Bittl, Freie Universität Berlin, Arnimallee 14, Berlin-Dahlem 14195, Germany

[5] Department of Physics and College of Optics and Photonics, University of Central Florida, 4111 Libra Drive, FL 32816-2385 Orlando, USA

Introduction

Poly(*N*-isopropylacrylamide) (PNIPAM) features thermoresponsive behavior in aqueous solution and a lower critical solution temperature (LCST) [1]. At atmospheric pressure, its cloud point T_{cp} is ca. 32 °C. In the one-phase state below T_{cp}, structural studies of semi-dilute PNIPAM solutions in D_2O using small-angle neutron scattering (SANS) revealed the presence of concentration fluctuations [2, 3]. The related static correlation length and the susceptibility were found to follow scaling behavior with respect to temperature. The resulting scaling exponents are slightly, but consistently lower than the ones predicted by mean-field theory, and this discrepancy was attributed to the hydrogen bonding of PNIPAM with water. Furthermore, it was found that, far below the critical (or spinodal) temperature T_c, water is a good solvent, while theta conditions are reached when approaching T_c [4]. Theoretical work [5] and quasi-elastic neutron scattering (QENS) pointed towards the importance of water molecules binding to the chains [6, 7]. These molecular processes may be expected to have an influence on the dynamics of the entire chain.

Dynamic light scattering (DLS) on semi-dilute aqueous PNIPAM solutions (up to a few wt% of PNIPAM) has revealed that the collective dynamics comprise two diffusive relaxation processes [8, 9]. The fast process was attributed to the relaxation of chain segments between neighboring overlap points. The associated dynamic correlation length was in the range of a few nanometers and was attributed to the distance between overlap points of the chains or, equivalently, to the cooperative motion of chain segments within the blobs [9]. The dynamic correlation lengths of the slow mode are of the order of a few 100 nm and were attributed to long-range concentration fluctuations [9]. Since this mode is only present in PNIPAM solutions in H_2O and in D_2O, but not in PNIPAM solutions in tetrahydrofuran, it was concluded that intermolecular interactions between PNIPAM chains through H_2O (or D_2O) bonds are at the origin of the slow mode [8]. The behavior in H_2O and in D_2O was very similar, except for small shifts of T_{cp} and the correlation lengths [8]. In a subsequent study using topologically constrained chains to exclude reptation mechanisms, the slow mode was assigned to the relaxation of correlated blobs [10]. In our previous DLS study on a 25 wt% solution of PNIPAM in D_2O, these two dynamic modes were observed as well, with the relative amplitude of the slow mode being very high [11]. Critical scaling of the dynamic correlation length could be confirmed, and an exponent of 0.67, characteristic of 3D Ising behavior, was found to describe the data better than scaling with the mean-field value of the exponent of 0.50. This deviation from mean-field behavior was attributed to pronounced large-scale heterogeneities. However, it should be kept in mind that, in general, the dynamic correlation length may be different from the static one. Especially for large values of the correlation length, deviations were encountered in semi-dilute and concentrated polymer solutions under theta conditions [12, 13].

The addition of a cosolvent, e.g., short-chain alcohol such as methanol, was shown to reduce the cloud point and to alter the hydration behavior of the PNIPAM chain in aqueous solution [14–18]. In dilute solution, the chain conformation in water/alcohol (methanol or ethanol) mixtures changes from expanded to collapsed, as cosolvent is added successively to the aqueous PNIPAM solution up to a certain volume fraction, where demixing sets in [19–21]. The dynamics of the PNIPAM chain and of the solvent molecules were found to be sensitively affected by a cosolvent, as found using broadband dielectric spectroscopy [22]. At room temperature, a number of relaxation processes were noted, namely the global motion of the chain, the local motion of the backbone, the motion of the side group, and the dipole orientation of the solvent molecule. Upon increasing the molar fraction of methanol from 0 to 0.15 (the case considered in the present work as well), the PNIPAM chains were found to contract, and the solvation unit that solvates PNIPAM is composed of one water molecule. Thus, the composition of the solvation shell of the polymer is of importance for the cononsolvency effect [23–26]. Our DLS measurements on a 25 wt% solution of PNIPAM in a 90:10 v/v and in an 85:15 v/v mixture of D_2O/CD_3OD revealed that the addition of methanol results only in minor changes compared to the solution in neat D_2O, the most prominent one being that the amplitude of the slow mode is slightly lower than in neat D_2O [11].

The phase behavior and chain conformation of PNIPAM in neat water not only depend on temperature, but also on pressure. In the temperature–pressure frame, the coexistence line of aqueous PNIPAM solutions is an ellipse with the pressure of the maximum being located in the range of 30–70 MPa for different molar masses, a wide concentration range and for both, H_2O and D_2O as a solvent, with the maximum value of the cloud point being a few Kelvin above the value at atmospheric pressure [27–31]. The origin of this non-monotonous behavior lies in the specific volume of the hydrated PNIPAM chain [32, 33]. In the one-phase region, an isothermal increase of pressure leads to an increase of the size of an individual PNIPAM chain and a subsequent decrease, as found in atomistic simulations [34]. QENS on a concentrated PNIPAM solution in D_2O revealed that, at temperatures below T_{cp}, the mean-square displacement of the local vibrational motions of the chain segments decreases with increasing pressure [29]. Using DLS on the equivalent solution in H_2O, fast and slow modes were observed in the one-phase state, and the dynamic correlation length deduced from the fast mode (related to the blob size) was found to increase from ca. 4.5 to 6.1 nm, as pressure was increased from 0.1 to 100 MPa [29]. These measurements were carried out at 15 °C, i.e., far away from the coexistence line. From these results, the authors concluded that the hydrogen bonds between PNIPAM and water are weakened by applying pressure in the one-phase state. In our recent QENS study on a 25 wt% solution of PNIPAM in H_2O, we found that the residence time of the hydration water at 130 MPa is lower than at atmospheric pressure, which confirms that the hydration interactions are pressure dependent [7].

In the presence of cosolvents, the coexistence lines of PNIPAM appear elliptical as in neat water, but the maxima are strongly shifted to higher pressure and temperatures (e.g., to ~230 MPa and ~40 °C in a 3 wt% solution of PNIPAM in 80:20 v/v D_2O/CD_3OD), and the one-phase region extends to significantly higher pressure [35–37]. The temperature-induced collapse of PNIPAM nanogels could be reversed by excess hydrostatic pressure, and it was found that pressure favors hydrogen bonds between PNIPAM and water to the cost of PNIPAM/methanol bonds [38]. In theoretical investigations and molecular dynamics simulations, the breakdown of cononsolvency at high pressure was attributed to the suppression of the cosolvent preferential solvation of

the polymer backbone at a rather high pressure imposed [26, 39, 40]. The pressure dependence of the chain conformation of a 3 wt% PNIPAM solution in an 80:20 v/v D_2O/CD_3OD mixture was recently studied by us using SANS [37]. In the one-phase state, we observed concentration fluctuations at small length scales, which show critical behavior with exponents far lower than predicted by mean-field theory. This deviation was attributed to large-scale inhomogeneities that are present already in the one-phase state. With increasing pressure, the exponent ν, that is deduced from the correlation length, increases and levels off above 150 MPa.

The effect of pressure on the chain dynamics in aqueous PNIPAM solutions containing cosolvent has, to the best of our knowledge, not been explored. A number of studies focused on the local dynamics at elevated pressure, though. Employing Raman spectroscopy to assess the vibrational dynamics of PNIPAM segments in neat water, we found that, at high pressure, the chains are more hydrated [41]. Subsequently, we used Raman spectroscopy and QENS to characterize the dynamics in PNIPAM solutions in an 80:20 v/v H_2O/CD_3OD mixture at 200 MPa [24]. In the one-phase region, i.e., below T_{cp}, the relative population of hydration water is equal at a pressure of 0.1 and 200 MPa and decreases weakly with increasing temperature. However, at 200 MPa, the relaxation time of hydration water becomes shorter, and it is more weakly bound, pointing to enhanced hydrophobic hydration at the expense of the hydration of hydrophilic groups. In the one-phase state, the mean-square displacement is lower at 200 MPa than at atmospheric pressure, which suggests that the altered hydration state at high pressure leads to chain stiffening. These changes in the local environment of the chain with pressure lead us to expect alterations in the chain dynamics and thus the collective dynamics.

DLS is sensitive to changes in the chain conformation and to dynamic large-scale inhomogeneities [42, 43] and is compatible with a high-pressure environment. While high-pressure DLS was previously used to investigate the effect of pressure on simple liquids [44, 45], glass formers [46], colloidal dispersions [47], polymer melts and blend [48, 49], protein solutions [50], micellar solutions [51, 52], and dispersions of thermoresponsive microgels [53], high-pressure DLS investigations on polymer solutions are scarce [54]. The latter investigation addressed the dynamic virial coefficient of a polymer in various solvents and thus the molecular origin of the respective solvent quality. Here, we employ high-pressure DLS to investigate the collective dynamics of concentrated solutions (25 wt%) of PNIPAM in water and in an 80:20 v/v water/methanol mixture. In previous DLS studies on PNIPAM solutions in water or water/methanol, extremely dilute [55, 56] or semi-dilute solutions [9] were investigated at atmospheric pressure only. Here, we address concentrated PNIPAM solutions and carry out pressure and temperature scans in the one-phase state, complementing our recent high-pressure SANS and QENS investigations on these systems [24, 37, 41].

Experimental section

Materials

PNIPAM (molar mass 36 kg/mol, Đ = 1.26) was purchased from Sigma-Aldrich. Deionized water, H_2O, D_2O and perdeuterated methyl alcohol-d4, CD_3OD (the two latter from Deutero GmbH) were used as solvents. PNIPAM was dissolved at a concentration of 25 wt% in neat D_2O, in neat H_2O or in an 80:20 v/v mixture of H_2O and CD_3OD. The solutions were shaken for at least 24 h at room temperature and then kept in the fridge. This polymer concentration and these solvents were used for consistency with previous experiments [7, 11, 24].

Cloud point determination

The cloud point temperatures T_{cp} were determined by monitoring the transmitted light intensity in situ in the DLS setup during a variation of pressure or during heating, in all cases coming from the one-phase state. The cloud point was determined from the decrease of the transmitted intensity.

Dynamic light scattering (DLS)

For DLS experiments at ambient and high pressure, a 35-mW HeNe laser ($\lambda = 632.8$ nm) was directed into the high-pressure sample cell by means of a mirror. The scattered light was recorded using an ALV/SO-SIPD photomultiplier to which the signal was fed by an optical fiber. A scattering angle $\theta = 70°$ was chosen. The intensity autocorrelation functions $G_2(\tau)$ were calculated by an ALV-5000/E correlator software. All parts were from ALV-Laser-Vertriebsgesellschaft mbH, Langen, Germany. Sample solutions were mounted in flasks from quartz glass having a diameter of 10 mm. These were sealed with a flexible Teflon cap to separate the sample from the pressure-transmitting medium. The flasks were installed in a custom-made, stainless steel, high-pressure chamber from SITEC equipped with sapphire windows in a Bridgman seal configuration. Toluene served as a pressure-transmitting and index-matching fluid. The pressure was generated with a SITEC hand spindle. The pressure was measured with a Brosa EBM 6045 transducer close to the inlet to the chamber. The pressure change during the measurements was negligible, even at the highest pressure used (1 MPa loss during the measurements at 200 MPa). The chamber temperature was controlled by a Julabo F12

thermostat and recorded by a Pt100 resistance attached to the outside of the pressure cell. It was calibrated by means of a Pt100 resistance inside the cell. Temperature scans at 0.1 MPa, 130 MPa, and 200 MPa were carried out 2–4 times. At each temperature, 10 measurements with a duration of 35 s were conducted, and each temperature scan was repeated thrice. Noisy measurements were discarded, and at each temperature, an average intensity autocorrelation function $G_2(\tau)$ was calculated from the remaining data. Close to the phase boundary, the incoming flux was reduced to avoid detector overload.

Angle-dependent measurements were carried out on the 25 wt% solution of PNIPAM in D_2O using the same DLS instrument. Instead of the high-pressure cell, the sample cell of the ALV instrument was used at atmospheric pressure. Its temperature was kept at 25 °C by a Julabo F32 thermostat. θ was varied between 15 and 155°. At each angle, 2 measurements having a duration of 60 s each were carried out.

The averaged $G_2(\tau)$ data were analyzed by inverse Laplace transformation (ILT) using the routine REPES [57] which calculates the distribution function of relaxation times, $\tau A(\tau)$ vs. $\log(\tau)$. The mean relaxation times of each mode were extracted as the centers of mass of the peaks. For the angle-dependent measurement, the relaxation rate $\Gamma = 1/\tau$ was plotted vs. the square of the momentum transfer $q = 4\pi n \sin(\theta/2)/\lambda$ (n is the refractive index of the solvent, see below), revealing linear behavior for the fast mode. Thus, the diffusion coefficients D of the fast mode were calculated for all samples by

$$D = \Gamma q^{-2} \tag{1}$$

from which the dynamic correlation lengths, ξ_{fast}, were obtained via the Stokes–Einstein relation,

$$\xi_{fast} = \frac{k_B T}{6\pi\eta D} \tag{2}$$

Here, k_B denotes Boltzmann's constant, T the absolute temperature and η the temperature-dependent viscosity of water. In the investigated pressure range, the refractive index of water does not change by more than 2% [58]. Thus, the temperature-dependent refractive indices at atmospheric pressure were used throughout. The results of first- or second-order polynomial fits are given in Table 1.

For normalization, the $G_2(\tau)$-1 data were divided by the amplitude of the model fit at 0.01 ms, giving $g_2(\tau)$-1. This way, artifacts from a randomly occurring very fast decay, that is presumably due to noise, are avoided.

The viscosity of water does not change by more than 5% in the investigated pressure and temperature range [61]. Therefore, it was assumed to be pressure independent, and only its temperature dependence was considered.

Table 1 Refractive indices used

Sample	Refractive index n
D_2O	$1.246 \pm 0.019 + (6.4 \pm 1.3) \times 10^{-4}$ K^{-1} T $-$ $(1.21 \pm 0.20) \times 10^{-6}$ K^{-2} T^2 [a]
H_2O	$1.217 \pm 0.008 + (8.7 \pm 0.5) \times 10^{-4}$ K^{-1} T $-$ $(1.62 \pm 0.09) \times 10^{-6}$ K^{-2} T^2 [b]
80:20 v/v H_2O/CD_3OD	$1.370 \pm 0.001 - (1.32 \pm 0.04) \times 10^{-4}$ K^{-1} T [c]

(a) From ref [59]. (b) From ref [60]. (c) Measured using an Abbe refractometer. Temperatures are given in K

The temperature-dependent viscosities of H_2O and D_2O at atmospheric pressure were calculated as described in refs [62] and [63], respectively. To determine the temperature-dependent viscosities of the 80:20 v/v H_2O/CD_3OD 80:20 v/v mixture, the viscosities of H_2O and of the 80:20 v/v H_2O/CD_3OD mixture were determined at 0.1 MPa using silica nanospheres from NanoComposix (Prague, Czech Republic), as described in the Supporting Information (SI). These values were used at all pressures.

Results and discussion

In this section, we present the results from DLS measurements on a 25 wt% PNIPAM solution in neat D_2O in dependence on pressure at a temperature of 34.0 °C, i.e., close to the maximum of the coexistence line. To determine the effect of pressure on the temperature-dependent scaling behavior of the dynamic correlation length, temperature scans were carried out using 25 wt% PNIPAM solutions in H_2O and in an 80:20 v/v H_2O/CD_3OD mixture at a pressure of 0.1, 130, and 200 MPa. These solvents were chosen to enable an unambiguous comparison of the results with the ones from our recent QENS study on the same sample, which focused on water dynamics [41].

Phase behavior

The phase diagram of the PNIPAM solutions is shown in Fig. 1. The transition pressures of the 25 wt% PNIPAM solution in D_2O, measured in pressure scans at various temperatures, coincides with the cloud points T_{cp} from solutions in H_2O, i.e., the change of solvent does not appear to play a role in the phase behavior. Fitting an ellipse was not feasible, because of the low number of data points and the small portion of the ellipse, that was covered. To determine the maximum of the coexistence line, a parabola was fitted to the combined data set, which gives a good fit in the range considered, as shown previously [30]. The fitting parameters are given in Table 2. The maximum is located at 78 MPa and 35.8 °C, which is 3.1 °C
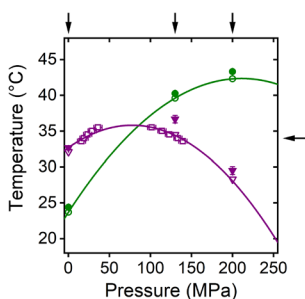
Fig. 1 Phase diagram of PNIPAM in aqueous solutions and in an 80:20 v/v water/methanol mixture. Open symbols: cloud points T_{cp} of the 25 wt% PNIPAM solution in D_2O (purple squares), in H_2O (purple triangles down), and in an 80:20 v/v H_2O/CD_3OD mixture (olive circles) from turbidimetry. Full lines: fits of parabolas to the cloud points in D_2O and H_2O (purple) and in the 80:20 v/v H_2O/CD_3OD mixture (olive). The one-phase regions are located at temperatures below the lines, the two-phase regions above. Arrows indicate the temperature and the pressures chosen for the pressure and the temperature scans. Closed symbols: critical temperatures T_c, same symbols and colors as for T_{cp}

Table 2 Fitting parameters of the coexistence lines

Sample	p_{max} (MPa)[a]	T_{cp}^{max} (°C)[b]	T_{cp} at 0.1 MPa (°C)
25 wt% PNIPAM in H_2O or D_2O	77.6	35.8	32.7
25 wt% PNIPAM in 80:20 v/v H_2O/CD_3OD	203	40.9	23.7

(a) Pressure and (b) temperature of the maximum of the parabola

higher than at 0.1 MPa. The temperature for a pressure scan was chosen at 34 °C; at this temperature, the left and the right branch of the coexistence line are located at 18.5 and 137 MPa, respectively.

For the PNIPAM solution in the 80:20 v/v H_2O/CD_3OD mixture, T_{cp} values were determined in heating scans and were found at 23.7, 39.6, and 42.3 °C at the 3 pressures of 0.1, 130, and 200 MPa, respectively (Fig. 1). Fitting a parabola to these data points, the maximum of the coexistence line is
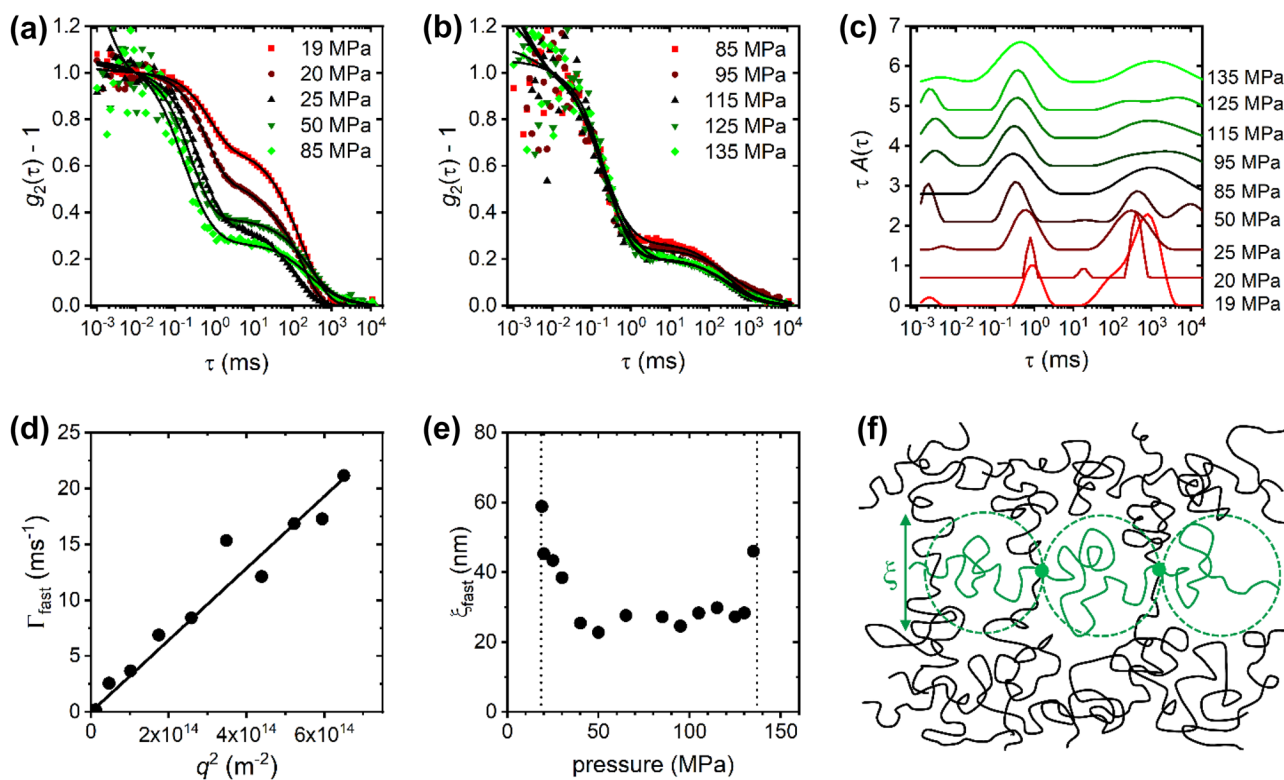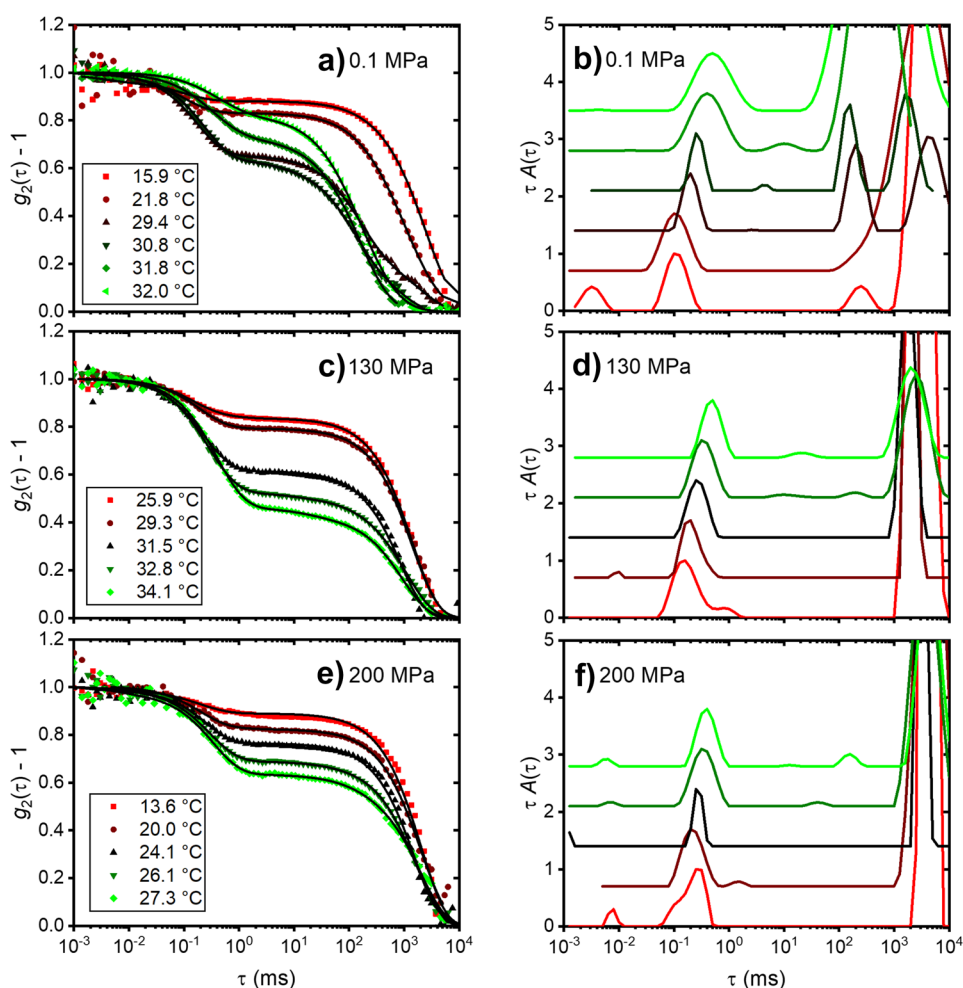

Fig. 2 Dynamics of the PNIPAM solution in H_2O. **a, b** Representative normalized intensity autocorrelation functions $g_2(\tau)-1$ at 34.0 °C and $\theta = 70°$ at low (**a**) and high pressures (**b**), as indicated in the graphs. Symbols: experimental data, lines: fitting functions obtained by REPES. For clarity, only every second experimental data point is shown. **c** Corresponding distribution functions of relaxation times in equal area representation, namely $\tau A(\tau)$ vs. τ on a logarithmic scale. The curves were normalized to the height of the fast peak and shifted vertically. **d** Relaxation rates of the fast mode in dependence on q^2 at 25 °C and 0.1 MPa. **e** Dynamic correlation length of the fast mode, ξ_{fast}, at 34.0 °C in dependence on pressure. The vertical dashed lines indicate the locations of the left and the right branch of the coexistence line at this temperature. **f** Schematic structure of the concentrated polymer solution with the correlation length ξ. A representative chain is colored in green. Dashed circles indicate the blobs

Fig. 3 Temperature-dependent dynamics of the PNIPAM solution in H$_2$O at various pressures. **a, c, e** Representative normalized intensity autocorrelation functions $g_2(\tau)$-1 at 0.1 MPa (**a**), 130 MPa (**c**), and 200 MPa (**e**) at the temperatures given in the graphs. Symbols: experimental data, lines: fitting functions obtained by REPES. For clarity, only every second experimental data point is shown. The autocorrelation functions were normalized by the intercept of the fitting function. **b, d, f** Corresponding distribution functions of relaxation times in equal area representation. The curves were normalized to the height of the fast peak and shifted vertically

obtained at 203 MPa and 40.9 °C, while the cloud point at 0.1 MPa is 23.7 °C (Table 2). Thus, the coexistence line is shifted to a significantly higher pressure than in neat water, as shown previously on a more dilute solution [37].

The pressures for the temperature-resolved DLS measurements were chosen on the left (0.1 MPa) and on the right side of the maximum (130 and 200 MPa) for the 25 wt% PNIPAM solution in H$_2$O, but lie all on the left side of the maximum for the one in H$_2$O/CD$_3$OD. We note that both coexistence lines are slightly shifted and distorted compared to the ones of 3 wt% solutions [31, 37], pointing to the importance of interchain interactions.

Pressure-dependent dynamics of the PNIPAM solution in neat water

Figure 2 shows the normalized intensity autocorrelation functions $g_2(\tau)$-1 of the 25 wt% PNIPAM solutions in neat D$_2$O at 34.0 °C at a pressure between 19 and 135 MPa, all measured at $\theta = 70°$. Two decays are consistently observed,

namely a fast one around 0.1–1 ms and a slow one around 10^2 ms. The fast and the slow mode reflect the relaxation of chain segments between overlap points (or inside the blobs) and long-range concentration fluctuations (or the relaxation of correlated blobs), respectively [10]. The relative area of the slow process deduced from the peaks in the distribution functions is rather high at low pressure (~0.8 at 19 MPa) and decreases to ~0.43–0.53 at 65–135 MPa. The two decays are reflected in two peaks in the distribution functions of relaxation times, $A(\tau)$ (Fig. 2c). Note that we use the equal area representation, $\tau A(\tau)$. The fast one is rather narrow and moves to smaller relaxation times τ with pressure increasing to 50 MPa, then becomes pressure independent. At the same pressure, the peak related to the slow mode becomes broad and is only partially present in the time window. While this hampers a quantitative analysis of the slow mode, it seems that the relaxation of the blobs becomes more broadly distributed, as pressure is increase. This might be attributed to a weakening of interchain interactions [10].
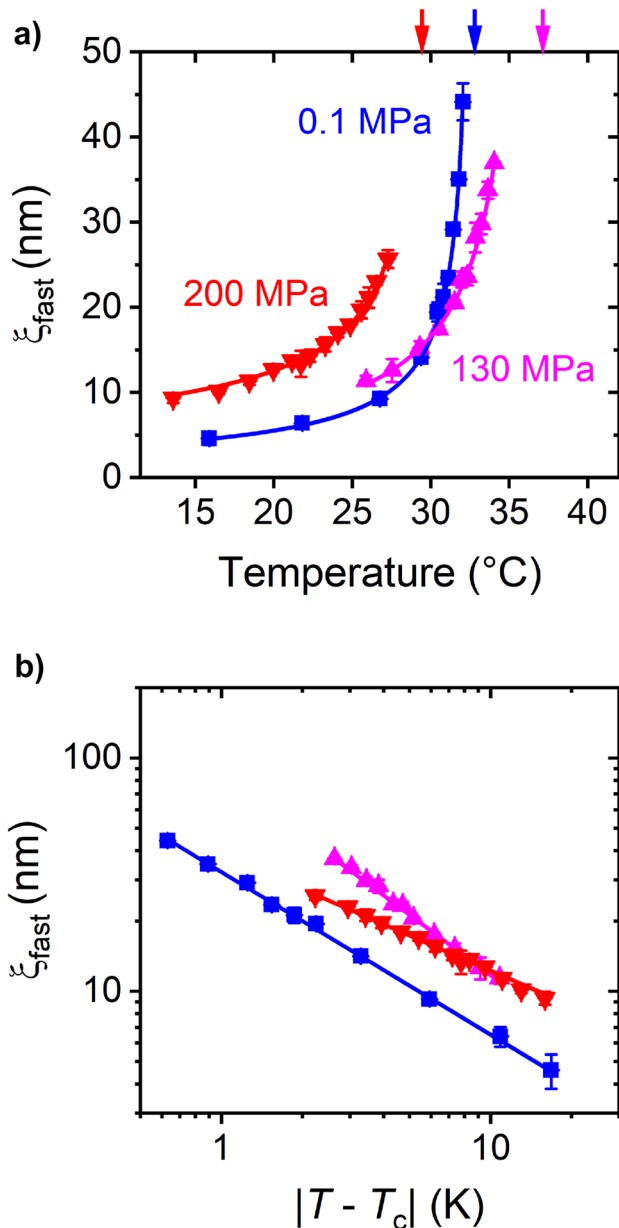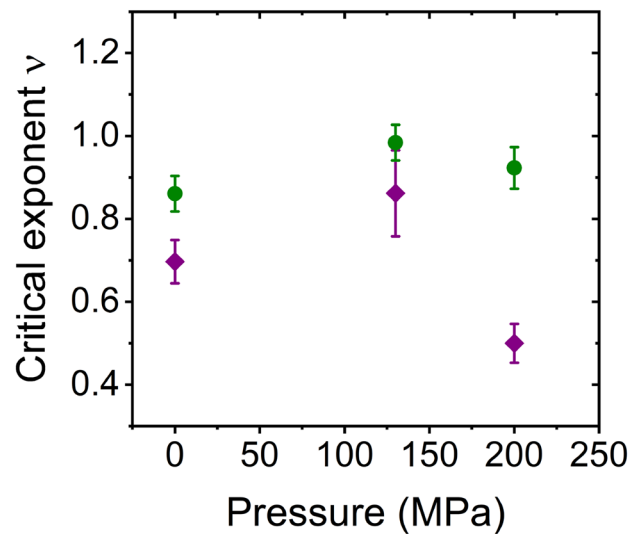
Fig. 5 Critical exponents ν for the fast mode in the PNIPAM solution in H_2O (purple diamonds) and in 80:20 v/v H_2O/CD_3OD (olive circles) in dependence on pressure

Fig. 4 Fast dynamic correlation length of the PNIPAM solution in H_2O for various pressures. **a** ξ_{fast} in dependence on the temperature at the pressure given in the graph. The arrows on the top indicate the pressure-dependent cloud points T_{cp}. **b** Same data in the form of ξ_{fast} vs. $|T - T_c|$, where T_c is the critical temperature determined from the fit of Eq. (3)

similar to the ones of ~4–6 nm found previously at similar temperatures on solutions having similar PNIPAM concentrations [11, 30].

The pressure dependence of the dynamic correlation length ξ_{fast} calculated from the relaxation times of the fast mode at 34.0 °C (Fig. 2c) is shown in Fig. 2e. ξ_{fast} decreases from ca. 59 nm at 19 MPa to ca. 23 nm at 50 MPa and increases again closely to the phase transition pressure at high pressure to ~46 nm at 135 MPa, i.e., non-monotonous behavior is observed. ξ_{fast} reflects the distance between the transient overlap points of the chains or, equivalently, the size of the blobs. Its increase towards the left and right branches of the coexistence line may be attributed to the incipient collapse of the chains or segments thereof, which results in an overall increase in distance between chain segments, in line with results from molecular dynamics simulations [34]. The slow mode becomes more intense upon approaching the left branch of the coexistence line, i.e., large-scale fluctuations become more prominent. As shown previously, an increased amplitude of the slow mode can be a result of the dynamic coupling of the two relaxation processes, which occurs when the relaxation times of both processes approach each other [64]. As is observed in Fig. 2c, the relaxation times of the fast and the slow mode are relatively close at low pressure. This is not the case, when pressure is increased to 135 MPa. Thus, at high pressure, the solution stays more homogeneous at large length scales. We note that the behavior near the left branch of the coexistence line was not captured in the earlier DLS study, where the pressure effect was investigated at 15 °C, i.e., far from the coexistence line [30].

Angle-dependent measurements on the solution at 25 °C and 0.1 MPa, i.e., in the one-phase region, reveal, that the relaxation rate Γ of the fast mode is proportional to q^2 (Fig. 2d), in consistency with previous results on a similar sample [11]. Using Eqs. (1) and (2), a dynamic correlation length $\xi_{fast} = 6.4$ nm is calculated from the slope of the fit. This value is
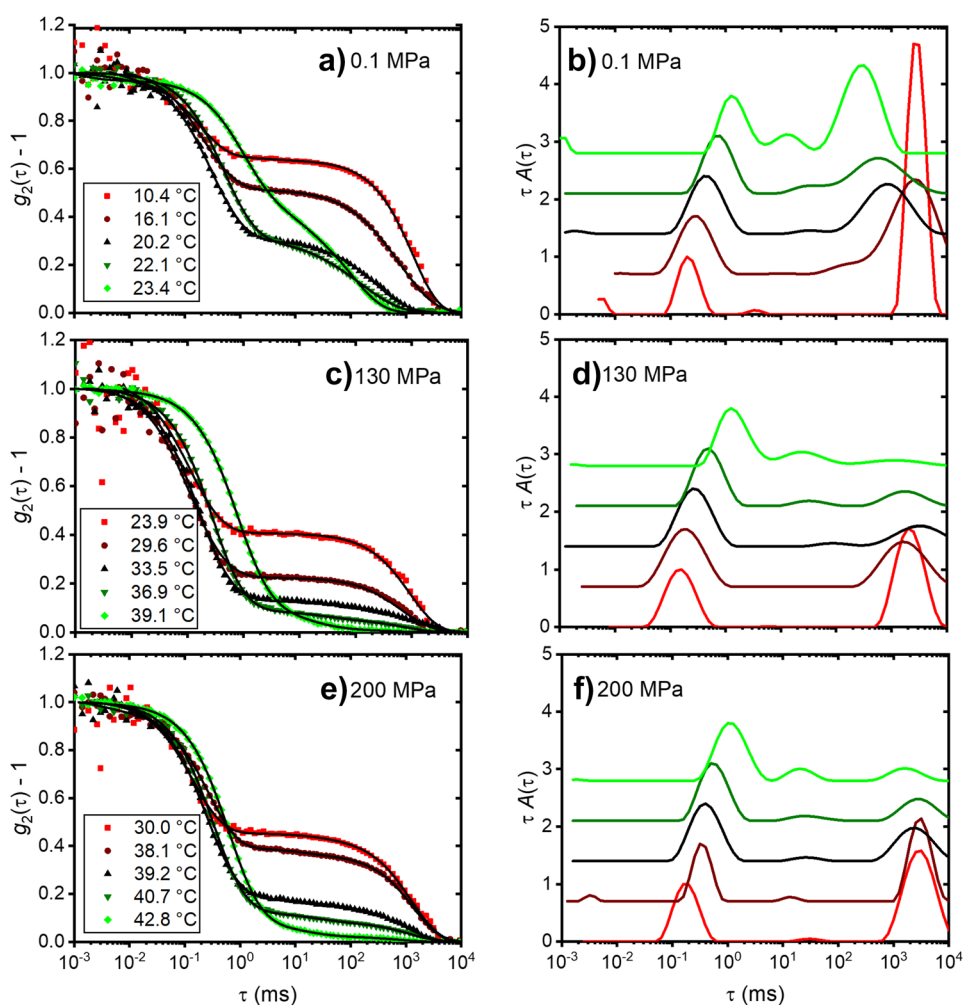
Fig. 6 Temperature-dependent dynamics of the PNIPAM solution in 80:20 v/v H$_2$O/CD$_3$OD at various pressures. **a, c, e** Representative normalized intensity autocorrelation functions $g_2(\tau)$-1 at 0.1 MPa (**a**), 130 MPa (**c**), and 200 MPa (**e**) at the temperatures given in the graphs. Symbols: experimental data, lines: fitting functions obtained by REPES. For clarity, only every second experimental data point is shown. The autocorrelation functions were normalized by the intercept of the fitting function. **b, d, f** Corresponding distribution functions of relaxation times. The curves were normalized to the height of the fast peak and shifted vertically

Temperature-dependent dynamics of the PNIPAM solution in neat water

To characterize the dynamics in the different regimes in more detail, temperature scans were carried out at 0.1, 130, and 200 MPa in the one-phase region. These allow us to determine critical exponents, which are indicative of the mechanisms at play. We expect non-mean-field behavior at 0.1 MPa, while the reduction of large-scale fluctuations might lead to more mean-field-like behavior at 130 and 200 MPa.

Figure 3 shows the normalized intensity autocorrelation functions $g_2(\tau)$-1 of the 25 wt% PNIPAM solution in neat H$_2$O for the 3 pressures under investigation. For normalization, the $G_2(\tau)$-1 data were divided by the intercept of the model fit. At 0.1 MPa, two decays are consistently observed, namely a fast one around 0.1–1 ms with no clear trend and a slow one around 10^2–10^4 ms. The relative amplitude of the slow process is rather high at low temperatures (~0.9 at 15.9 °C) and decreases to ~0.62 at 30.8 °C. Due to the increased thermal energy at high temperatures,

the blobs become less correlated, leading to a smaller amplitude of the slow process [10]. At even higher temperatures, it increases again to ~0.8 at 32.0 °C, i.e., close to T_{cp}. Simultaneously, the slow process becomes significantly faster (Fig. 3b). As discussed above, these effects are presumably due to the dynamic coupling of both processes [64]. At 130 and 200 MPa, similar behavior is observed (Fig. 3c, e), i.e., two decays in similar time ranges are present, but the amplitude of the slow mode decreases steadily, as temperature increases. We hypothesize that the increase of the amplitude is not observed, because, at 130 and 200 MPa, measurements were only carried out more than 1 K away from the critical temperature (see Fig. 4b below), where dynamic coupling plays a less important role. Overall, the relative amplitude of the slow mode is mode peaks at 200 MPa. The two decays are reflected in 2 peaks in the distribution functions (Fig. 3b, d, and f). It is seen that the slow mode is partially outside the accessible time window. Therefore, its relaxation time is not considered further.

Again, the dynamic correlation length ξ_{fast} is calculated using Eq. (2) (Fig. 4a). The values rise, as the respective

cloud point is approached. The following equation, characteristic of critical scaling was fitted to the data:

$$\xi_{\text{fast}} = \xi_0 \left(\frac{T_c - T}{T_c} \right)^{-\nu} \qquad (3)$$

where ξ_0 is a constant, T_c is the critical temperature, and ν is the critical exponent. The data can be well described by this equation (Fig. 4a) and follow a straight line in a double-logarithmic representation in dependence on $|T_c - T|$ (Fig. 4b). The resulting values of T_c are indicated in the phase diagram in Fig. 1 and lie at all pressures slightly above the cloud point temperatures, as expected. The exponent ν increases from 0.70 ± 0.06 at 0.1 MPa to 0.86 ± 0.11 at 130 MPa, then decreases to 0.50 ± 0.05 at 200 MPa (Fig. 5). For static correlation lengths, a value of 0.50 is expected for a mean-field like, homogeneous polymer solution, whereas a value of 0.67 is characteristic of 3D Ising behavior. In the present case, the exponent of the dynamic correlation length is close to the mean-field value at 200 MPa, whereas the value at 0.1 MPa is close to the 3D Ising case and the one at 130 MPa is even higher.

Temperature-dependent dynamics of a PNIPAM solution in water/methanol

The autocorrelation functions from the 25 wt% solutions of PNIPAM in 80:20 v/v H_2O/CD_3OD are shown in Fig. 6. The overall appearance is the same as in neat H_2O; however, the fractions of the slow mode are overall lower than in neat H_2O, in consistency with our previous observations at atmospheric pressure [11].

Again, the dynamic correlation length ξ_{fast} was calculated using Eq. (2) (Fig. 7a). For all pressures, the values increase, as the cloud point is approached, similar to the behavior in neat H_2O. Equation (3) was successfully fitted to the data (Fig. 7a, b). The resulting T_c-values lie at all pressures slightly above the cloud point temperatures, as expected (Fig. 1). The exponent ν increases from 0.86 ± 0.05 at 0.1 MPa to 0.98 ± 0.05 at 130 MPa and then decreases weakly to 0.92 ± 0.06 at 200 MPa (Fig. 5). These values follow the same trend as in neat H_2O, but are significantly higher throughout, i.e., further deviate from the mean-field value, which points to stronger heterogeneity than in neat H_2O. We note that this is in conflict with the lower fraction of the slow mode than in neat H_2O. Therefore, other mechanisms must play a role as well.

As compared to PNIPAM in neat H_2O (Fig. 4b), ξ_{fast} is larger in H_2O/CD_3OD (Fig. 7b) at similar values of $|T-T_c|$ at atmospheric pressure. Thus, in the one-phase state, the presence of methanol results in more contracted chain conformations. This is in agreement with previous studies on the cononsolvency effect at atmospheric pressure, where it was found that

the preferential adsorption of the cosolvent leads to an overall weaker solvation of the chains [18]. At 130 MPa, the preferential adsorption is less pronounced, causing the temperature-dependences relative to the respective cloud points to become very similar. This finding supports the conclusion of previous studies that, at high pressure, methanol is replaced by water on the PNIPAM chains [24, 26, 37, 39, 40]. Thus, PNIPAM interacts mainly with water in both systems. However, in the water/methanol mixture, the hydrophobic effect is weakened because
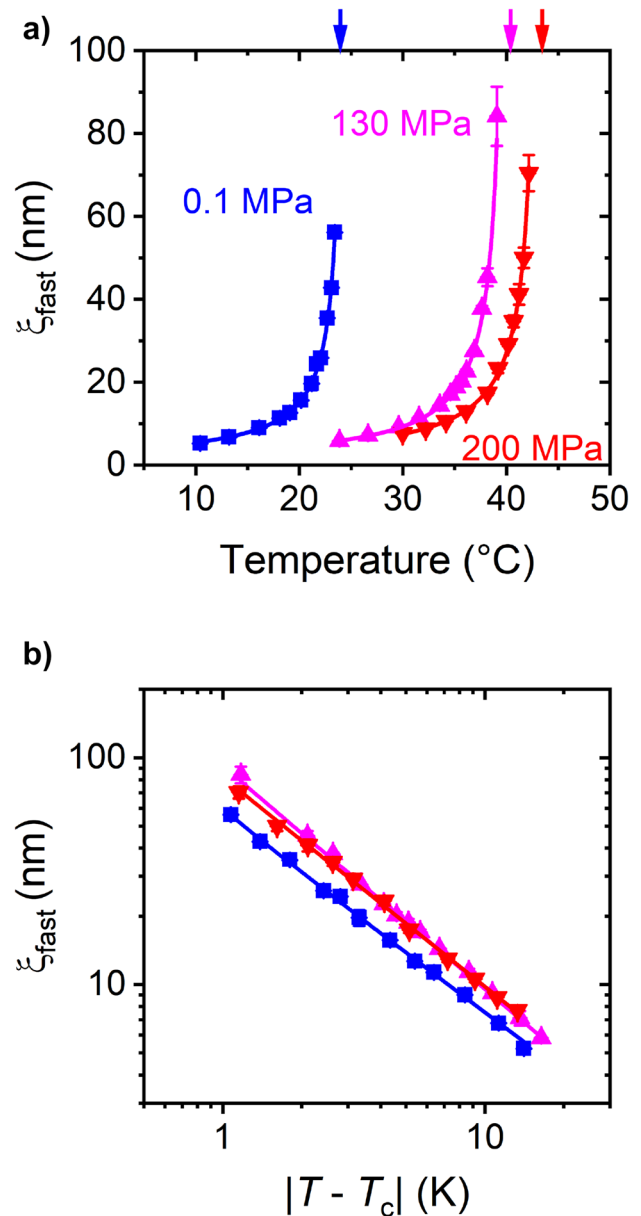

Fig. 7 Fast dynamic correlation length of the PNIPAM solution in 80:20 v/v H_2O/CD_3OD at various pressures. **a** ξ_{fast} in dependence on temperature at the pressure values given in the graph. The arrows on top indicate the pressure-dependent cloud points T_{cp}. **b** Same data in the form of ξ_{fast} vs. $|T - T_c|$

of the presence of methanol in the bulk solvent, leading to an increased T_{cp} as compared to the purely aqueous solution.

Furthermore, increasing pressure leads to larger values of ξ_{fast} for similar $|T\text{-}T_c|$ in both H_2O and H_2O/CD_3OD, which implies that, overall, the chains are more contracted at high pressure. This was also observed in a semi-dilute PNIPAM solution in water/methanol using SANS, probing the static correlation length [37]. Moreover, it was argued that a contracted chain conformation of PNIPAM in a mixture of water and methanol at high pressure is crucial for the origin of the observed stabilization of the one-phase state [26].

The obtained critical exponents are larger than those predicted by models. These were repeatedly observed for polymer solutions far from the critical temperature [65, 66]. This discrepancy may firstly be due to the presence of long-range interactions, i.e., interchain interactions, as evident from the pronounced slow decay indicating the presence of correlated blobs. Secondly, as discussed previously [37], the phase transition of PNIPAM at the coexistence line may be of weak first order, implying concentration fluctuations already before the transition [67, 68]. Mode-coupling between the fast and the slow mode, which could lead to different types of critical dynamics in polymer solutions [64], is expected to play only a minor role in the results presented here, as almost all measurements were carried out more than 1 K away from T_{cp}.

Conclusion

High-pressure DLS was successfully used to investigate the collective dynamics in concentrated solutions of the thermoresponsive polymer PNIPAM in water and water/methanol in the one-phase state. In neat water, two dynamic processes are observed, namely the fast relaxation of chains within the blobs and the slow relaxation of the cage formed by the surrounding blobs. The relative amplitude of the slow mode is rather high. At a temperature slightly below the maximum of the coexistence line in the temperature–pressure frame, the dynamic correlation length of the fast mode depends on pressure and features a minimum with a strong increase towards the left and the right branch of the coexistence line, which means that the chains contract. These findings are in accordance with the ones from atomistic simulations of a single chain [34].

Our temperature-dependent measurements of the PNIPAM solution in neat water at a pressure between 0.1 and 200 MPa reveal critical scaling behavior of the dynamic correlation length of the fast mode. The critical exponents of the dynamic correlation length are between 0.50 and 0.86 with a maximum value at a pressure of 130 MPa. The critical temperatures are found to lie slightly above the cloud point temperatures, as expected.

Temperature-dependent measurements of a PNIPAM solution in water/methanol result in similar behavior, albeit with higher values of the dynamic correlation lengths and higher critical exponents (0.86–0.98) than in neat water.

For solutions in water and in water/methanol, the dynamic correlation length increases with pressure, i.e., the chains contract. We attribute the overall high values of the critical exponents in both, neat water, and water/methanol, to the presence of long-range interactions, i.e., interchain interactions, and to fluctuations near the phase transition. Regardless of the solvent chosen, the maximum of the critical exponent is at 130 MPa, which seems unrelated to the maxima of the coexistence curves, that are vastly different in water and in water/methanol.

Availability of data and material N/A.

Code availability N/A.

Declarations

Competing interests The authors declare no competing interest.

References

1. Halperin A, Kröger M, Winnik FM (2015) Angew Chem Int Ed 54(51):15342–15367
2. Shibayama M, Tanaka T, Han CC (1992) J Chem Phys 97(9):6829–6841
3. Meier-Koll A, Pipich V, Busch P, Papadakis CM, Müller-Buschbaum P (2012) Langmuir 28(23):8791–8798
4. Kubota K, Fujishige S, Ando I (1990) Polym J 22(1):15–20
5. Okada M, Tanaka F (2005) Macromolecules 38(10):4465–4471

6. Philipp M, Kyriakos K, Silvi L, Lohstroh W, Petry W, Krüger JK, Papadakis CM, Müller-Buschbaum P (2014) J Phys Chem B 118(15):4254–4260

7. Niebuur B-J, Lohstroh W, Appavou M-S, Schulte A, Papadakis CM (2019) Macromolecules 52(5):1942–1954

8. Yu TL, Lu W-C, Liu W-H, Lin H-L, Chiu C-H (2004) Polymer 45(16):5579–5589

9. Yuan G, Wang S, Han CC, Wu C (2006) Macromolecules 39(10):3642–3647

10. Wang J, Wu C (2016) Macromolecules 49(8):3184–3191

11. Raftopoulos KN, Kyriakos K, Nuber M, Niebuur B-J, Holderer O, Ohl M, Ivanova O, Pasini S, Papadakis CM (2020) Soft Matter 16(36):8462–8472

12. Nicolai T, Brown W (1990) Macromolecules 23(12):3150–3155

13. Brown W, Nicolai T (1990) Colloid Polym Sci 268(11):977–990

14. Winnik FM, Ringsdorf H, Venzmer J (1990) Macromolecules 23(8):2415–2416

15. Schild HG, Muthukumar M, Tirrell DA (1991) Macromolecules 24(4):948–952

16. Costa ROR, Freitas RFS (2002) Phase Behavior of Poly(N-isopropylacrylamide) in Binary Aqueous Solutions. Polymer 43(22):5879–5885

17. Scherzinger C, Schwarz A, Bardow A, Leonhard K, Richtering W (2014) Curr Op Colloid Interf Sci 19(2):84–94

18. Bharadwaj S, Niebuur B-J, Nothdurft K, Richtering W, van der Vegt N, Papadakis CM (2022) Soft Matter 18(15):2884–2909

19. Zhang G, Wu C (2001) J Am Chem Soc 123(7):1376–1380

20. Chee CK, Hunt BJ, Rimmer S, Soutar I, Swanson L (2011) Soft Matter 7(3):1176–1184

21. Wang F, Shi Y, Luo S, Chen Y, Zhao J (2012) Macromolecules 45(22):9196–9204

22. Yang M, Zhao K (2017) J Polym Sci B: Polym Phys 55(16):1227–1234

23. Kyriakos K, Philipp M, Silvi L, Lohstroh W, Petry W, Müller-Buschbaum P, Papadakis CM (2016) J Phys Chem B 120(2):4679–4688

24. Niebuur B-J, Lohstroh W, Ko C-H, Appavou M-S, Schulte A, Papadakis CM (2021) Macromolecules 54(9):4387–4400

25. Tavagnacco L, Zaccarelli E, Chiessi E (2020) J Mol Liquids 297:111928

26. Budkov YA, Kolesnikov AL (2017) Soft Matter 13(45):8362–8367

27. Otake K, Karaki R, Ebina T, Yokoyama C, Takahashi S (1993) Macromolecules 26(9):2194–2197

28. Kunugi S, Yamazakim Y, Takano K, Tanaka N (1999) Langmuir 15(12):4056–4061

29. Shibayama M, Isono K, Okabe S, Karino T, Nagao M (2004) Macromolecules 37(8):2909–2918

30. Osaka N, Shibayama M, Kikuchi T, Yamamuro O (2009) J Phys Chem B 113(39):12870–12876

31. Niebuur B-J, Chiappisi L, Zhang X, Jung F, Schulte A, Papadakis CM (2018) ACS Macro Lett 7(10):1155–1160

32. Ohta H, Ando I, Fujishige S, Kubota K (1991) J Polym Sci B 29(8):963–968

33. Mochizuki K, Sumi T, Koga K (2016) Phys Chem Chem Phys 18(6):4697–4703

34. Tavagnacco L, Chiessi E, Zaccarelli E (2021) Phys Chem Chem Phys 23(10):5984–5991

35. Osaka N, Shibayama M (2012) Macromolecules 45(4):2171–2174

36. Ebeling B, Eggers S, Hendrich N, Nitschke A, Vana P (2014) Macromolecules 47(4):1462–1469

37. Niebuur B-J, Ko C-H, Zhang X, Claude K-L, Chiappisi L, Schulte A, Papadakis CM (2020) Macromolecules 53(10):3946–3955

38. Hofmann CH, Grobelny S, Erlkamp M, Winter R, Richtering W (2014) Polymer 55(8):2000–2007

39. De Oliveira TE, Netz PA, Mukherji D, Kremer K (2015) Soft Matter 11(44):8599–8604

40. Pica A, Graziano G (2017) Biophys Chem 231:34–38

41. Niebuur B-J, Claude K-L, Pinzek S, Cariker C, Raftopoulos KN, Pipich V, Appavou M-S, Schulte A, Papadakis CM (2017) ACS Macro Lett 6(11):1180–1185

42. Burchard W, Richtering W (1989) In: Pietralla M, Pechhold W (eds) Relaxation in Polymers. Progr Colloid Polymer Sci, vol 80. Steinkopff.

43. Nicolai T, Brown W (1996) In: Brown W (ed) Light Scattering. Principles and Development Clarendon Press, Oxford ch 5

44. Lilge D, Eimer W, Dorfmüller Th (1987) J Chem Phys 86(1):391–396

45. Meier G, Vavrin R, Kohlbrecher J, Buitenhuis J, Lettinga MP, Ratajczyk M (2008) Meas Sci Technol 19(3):034017

46. Paluch M, Patkowski A, Fischer EW (2000) Phys Rev Lett 85(10):2140–2143

47. Vavrin R, Kohlbrecher J, Wilk A, Ratajczik M, Lettinga MP, Buitenhuis J, Meier G (2009) J Chem Phys 130(15):154903

48. Fytas G, Meier G, Dorfmüller Th (1985) Macromolecules 18(5):993–996

49. Beiner M, Fytas G, Meier G, Kumar S (1998) Phys Rev Lett 81(3):594–597

50. Nyström B, Roots J (1983) J Chem Phys 78(6):2833–2837

51. Gebhardt R, Doster W, Friedrich J, Kulozik U (2006) Eur Biophys J 35(6):503–509

52. Kostko AF, Harden JL, McHugh MA (2009) Macromolecules 42(14):5328–5338

53. Wrede O, Reimann Y, Lülsdorf S, Emmrich D, Schneider K, Schmid AJ, Zauser D, Hannappel Y, Beyer A, Schweins R, Gölzhäuser A, Hellweg T, Sottmann T (2019) Sci Rep 8:13781

54. Kermis TW, Li D, Guney-Altay O, Park IH, van Zanten JH, McHugh MA (2004) Macromolecules 37(24):9123–9131

55. Wu C, Zhou S (1995) Macromolecules 28(24):8381–8387

56. Zhang G, Wu C (2001) Phys Rev Lett 86(5):822–825

57. Jakeš J (1995) Collect Czech Chem Commun 60(11):1781–1797

58. Waxler RM, Weir CE (1963) J Res Natl Bur Stand A. Phys Chem 67A(2):163–171

59. Odhner H, Jacobs DT (2011) J Chem Eng Data 57(1):166–168

60. Harvey AH, Gallagher JS, Levelt Sengers JMH (1998) J Phys Chem Ref Data 27(4):761–774 (Springer Data Base)

61. Horne RA, Johnson DS (1966) J Phys Chem 70(7):2182–2190

62. Huber ML, Perkins RA, Laesecke A, Friend DG, Sengers JV, Assael MJ, Metaxa IN, Vogel E, Mares R, Miyagawa K (2009) J Phys Chem Ref Data 38(2):101–125

63. Assael MJ, Monogenidou SA, Huber ML, Perkins RA, Sengers JV (2021) J Phys Chem Ref Data 50(3):033102

64. Kostko AF, Anisimov MA, Sengers JV (2007) Phys Rev E 76(2):021804

65. Kita R, Kubota K, Dobashi T (1997) Phys Rev E 56(3):3213–3218

66. Jacob J, Anisimov MA, Sengers JV, Dechabo V, Yudin IK, Gammon RW (2001) Appl Opt 40(24):4160–4169

67. Graziano G (2000) Int J Biol Macromol 27(1):89–97

68. Zhang Q, Weber C, Schubert US, Hoogenboom R (2017) Mater Horiz 4(2):109–116